2026 IEEE International Conference on Robotics and Automation (ICRA 2026)
June 1-5, 2026. Vienna, Austria

Investigation of Multiple Buoyancy Controller Equipped Underwater Glider Robot Modeling for Control System Development and Gliding Simulation

Luis Canete[1], Jun Paquibot[2], Masaharu Matsumoto[3], Takayuki Takahashi[4]

***Abstract*— This paper discusses the development of a model for an underwater glider robot equipped with multiple buoyancy controllers aimed at environmental surveying of lakes. Primary target of the model is performing 2D simulation of actual gliding that will lead to control system development. This proves to be a challenge as gliding requires calculation of hydrodynamic forces in the medium, in this case water, which typically involves Computational Fluid Dynamics (CFD). Although CFD is a well established technique, it's a well known fact that it is expensive both in terms of computational resources and valuable time. Instead, an approach that combines CFD with Euler-Lagrange equations is proposed and undertaken. Discussion regarding the proposed underwater glider, derivation of the model, the architecture of the simulation, and preliminary simulation results referenced with actual gliding results are presented.**

I. INTRODUCTION

In March 11, 2011, the Great East Japan Earthquake caused a tsunami that ravaged the north eastern coast of Japan which lead to the nuclear accident at the Daichi-Power Plant in Fukushima Prefecture. Since then, efforts have been made to perform environmental surveying of large lakes in the region aimed at measuring and assessing the radioactive contamination and its dynamics. To aid in performing risky surveying tasks, researchers from Fukushima University developed an underwater remotely operated vehicle (UROV). This UROV (Fig.1a) was aimed at reaching the lakebed to perform undisturbed mud core-sampling [1] by forcing a thin metallic pipe into the mud [2][3] at depths of up to 100 meters. While able to successfully sample a core, the UROV could only travel a distance of approximately 700 meters before needing to return for recharging or battery replacement. Clearly, this shows that the UROV is not efficient in terms of large area multi-location sampling needed to create a map of the radioactive particle distribution. Furthermore, the resulting small area coverage requires boats that would take the UROV to each location increasing cost, time and effort. Upon analyzing the shortcomings of the UROV, it was identified that the use of thrusters for propulsion was the root cause of its inefficiency for long distance travel. Due to the large drag force in water, thrusters need to constantly generate thrust to move from one point to another resulting in significant energy loss. An alternative to thruster equipped underwater vehicles is an underwater glider. Underwater gliders are equipped with a wing or hydrofoil and control their buoyancy to generate vertical motion. When sufficient flow of water over the surface of the wing occurs, lift is generated. With the right angle of attack, this lift will cause horizontal motion together with the vertical motion resulting in gliding. Due to the fact that controlling buoyancy requires lesser energy compared to thrusters, energy efficiency is achieved. It should be noted that the authors do not to intend to completely remove thrusters from the system but augment it with a gliding ability for energy efficient long distance travel. Thrusters, on the other hand, will be used for precise positioning and pose correction for certain tasks like the aforementioned mud core-sampling. However, in this paper focus is given solely to the gliding aspect of the proposed system.

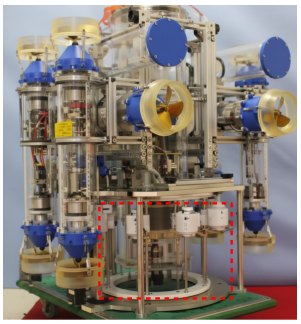

(a) Thruster-equipped UROV with 8-core Reloadable Core Sampling Module(in red box)

(b) Slocum Glider by Teledyne Webb Research Commercially Available System

Fig. 1: Thruster based underwater remotely operated vehicle and the industry standard underwater glider

A. An Underwater Glider for Surveying Lakes

There have been many implementations of underwater gliders as shown in a review by Khan [4] indicative of the interest in their unique features. In fact, commercially available underwater gliders like the Slocum Glider (Fig.1b) are used extensively in academic and industrial oceanic surveying as described in [5][6]. However, while having a wide array of sensing and sampling modules, these systems deviate from the current target capabilities the authors are consider-

*This work is supported by FREI

[1]Luis Canete, Faculty of Comp. Eng, School of Eng, Univ. of San Carlos, Philippines lscanete@usc.edu.ph

[2]Jun Paquibot, Grad Student of Comp. Eng, School of Eng, Univ. of San Carlos, Philippines 18103689@usc.edu.ph

[3]Masaharu Matumoto, Faculty of Symbiotic Sys Sci and Eng, Fukushima Univ., Japan matsumoto@sss.fukushima-u.ac.jp

[4]Takayuki Takahashi, Faculty of Symbiotic Sys Sci and Eng, Fukushima Univ., Japan taka@sss.fukushima-u.ac.jp

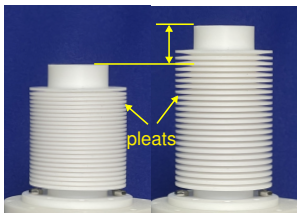

(a) Bellows type buoyancy controller

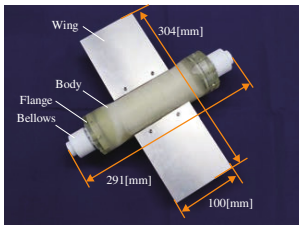

(b) Dual buoyancy controller equipped glider for gliding test

(c) Actual 2D gliding test of dual buoyancy controller equipped glider

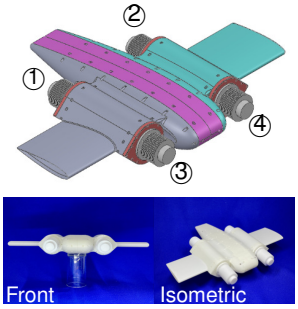

(d) Proposed quad buoyancy controller glider under development

Fig. 2: Baseline components for proposed underwater glider

ing. First and foremost, commercially available gliders are not readily capable nor are they designed with mud core-sampling in mind. The streamlined geometry of their outer shell is highly optimized and sampling modules are designed around this optimal shape. Therefore, any modifications like adding a core sampling module to the exterior may negatively impact gliding leading to undesirable performance. Secondly, most of these gliders are bulky reaching lengths of almost two meters and heavy at a minimum of 55 [kg] which may require teams of operators and specialists. Lastly, the extreme high pressure of the depths these gliders reach necessitates the use of oil bladders for their buoyancy controllers which is beyond the need for the targeted 100 meter depth of lakes and may be a key driver of the cost of these gliders. Taking these factors into consideration, the authors intend to develop an underwater glider that is intended for lakes with 100 meter maximum depths; small and lightweight that can be carried by two people; uses a simpler implementation of a buoyancy controller suited to the target depth; and incorporates mud core-sampling in its design.

B. Bellows Type Buoyancy Controller

A simpler buoyancy controller that the authors are adapting is shown in Fig.2a. This buoyancy controller uses PTFE machined to form bellows that are compliant. When the top of the structure is pushed from the inside, it expands increasing its volume. Such a design is indeed simpler as a linear actuator can easily be used to expand the bellows. A maximum of 0.4 [N] of buoyancy can been generated by the design [7] and has been tested to function up to pressures of 1 [MPa] without rupturing which corresponds to the target maximum depth of 100 [m]. In fact, researchers in [8] have used this design in a glider equipped with two buoyancy controllers, one each in the front and back. This gave the glider the ability to control its pitch angle up or down by creating a difference in the buoyancy of the front and back controllers effectively moving the center of buoyancy (CoB) away from alignment with the center of mass (CoM). Initial tests showed the gliding ability using the two buoyancy controllers.

C. Proposed Quad Buoyancy Equipped Glider

With the initial tests using the bellows showing basic gliding, the authors intend to extend the system from dual buoyancy controllers to quad buoyancy controllers as shown in Fig.2a. The arrangement of the four buoyancy controllers will enable roll and pitch angle control resulting in gliding with banking control allowing turning to the left and right. The authors consider this a unique departure from other designs [9][10] that use a buoyancy controller together with an internally movable mass to create rolling and pitching moments. The quad buoyancy controller approach uses a uniform input variable which is buoyancy instead of a mix of mass position and buoyancy. This may reduce the complexity of the control as the interactions between an internally moving mass and the glider frame is minimized.

D. The Challenge of Modeling the Proposed Glider

With the development of the prototype of the quad buoyancy controller underway, concerns regarding its modeling and resulting control have been raised. While finding the model will lead to a better understanding of the characteristics of the system, the primary concern of the authors is to be able to develop a control method for multiple buoyancy controller equipped gliders. To do this, the model will have to lead to simulation that can be used to not only analyze characteristics but develop control techniques rapidly.This proves challenging since most well established models of gliders seem to be based on the Slocum Glider or ones with similar shape like the Spray [11]. While some characteristics are the same, there are key differences. One obvious difference is the multiple buoyancy approach which changes both the volume and position of the CoB of each controller and is not accounted for in most models. Also, the general shape of the proposed system departs from the typical highly streamlined fuselage of most gliders since the buoyancy controllers are exposed. Additionally, the mud core sampling module will most likely be on the exterior so a streamlined outer geometry may not be strictly enforced in the design process. Furthermore, most of the models use an approach akin to Newton's method that identifies each force acting on the body individually and then summing them. While this is a widely accepted method, certain forces may be omitted especially in this case where the design is quite different from exising references.

TABLE I: Model Parameters

symbol	unit	description
x	[m]	position of glider in the x-axis
z	[m]	position of glider in the z-axis
θ	[rad]	pitch angle of glider
M	[kg]	mass of entire glider
I	[kgm^2]	moment of inertia of glider along its CoG
l_{gx}, l_{gz}	[m]	position of CoG in the body frame
$V_{0...2}$	[m^3]	volume of glider fuselage and buoyancy controllers
C_{33}	[Nms]	damping friction at the wheel axis
g	[m/s^2]	gravity acceleration

Another significant challenge is the incorporation of hydrodynamic forces and moments in the model. For irregular shapes as the one in the proposed glider, these forces and moments would require Computational Fluid Dynamics (CFD). However, CFD is computationally expensive in terms of memory resources and processing time. Simply combining the spatial domain of CFD with temporal domain of rigid body dynamics would result in extremely long processing per time step to be of any practical use.

II. MODELING MULTIPLE BUOYANCY CONTROLLER EQUIPPED GLIDERS

An approach that the authors are pursuing involves using the parametric approach of Lagrangian Mechanics and the Euler-Lagrange equations of motion to enable the representation of multiple buoyancy controllers. This also encapsulates the individual change in the buoyancy and CoB of each controller. Furthermore, any additional components could be easily added to the model by identifying its mass, volume and position in the design.

To incorporate hydrodynamic forces, CFD could be used calculate and record the forces and moments at relevant poses and velocities a priori. These values could be used in an interpolating function like a polynomial to retrieve intermediate values. This would allow trivial computation of the forces and moments that could be incorporated into the simulation of the equations of motion.

As an initial step and verification of this method, a 2D model that incorporates a multiple buoyancy controller design will be developed. In particular, the vertical plane of the glider is considered which focuses on pitching, forward and downward motion. Although this reduces the 3D nature of the quad buoyancy feature, the authors believe this to be a reasonable first step for modeling multiple buoyancy controller equipped gliders since these dimensions capture gliding ability. This is of importance when trying to develop a control that maximizes horizontal displacement during gliding. Once this method has been found to be in coherence with actual two dimensional gliding (Fig.2c), focus will then shift to three dimensional gliding and a 3D model.

And so, for the derivation and the analysis that will follow, the dual buoyancy equipped glider shown in Fig.2b will be used. Once this is validated, adding more dimensions and

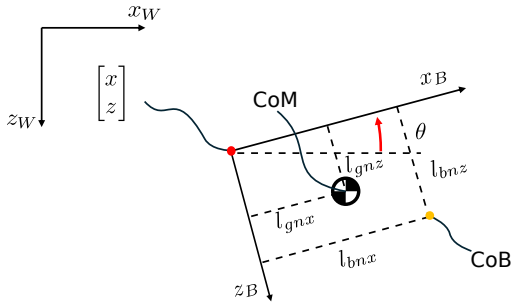

(a) Coordinate frame assignment and kinematic relationship of rigid body components

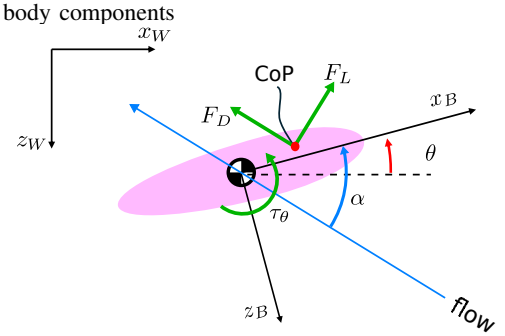

(b) Hydrodynamic forces and moment and angle of attack

Fig. 3: Identifying parameters and establishing kinematic relationship of forces

degrees of freedom (DOF) will follow for the quad buoyancy controller equipped glider.

A. 2D Parameterized Rigid Body Dynamics

Derivation of the rigid body dynamics of the glider start with assuming a fixed coordinate frame x_W-z_W and a body attached coordinate frame x_B-z_B (Fig.3a). A point $\mathbf{P}_B = [P_x, P_z]^\top$ defined on the x_B-z_B axis could be transformed into a point $\mathbf{P}_W$ on the x_W-z_W axis through

$$\mathbf{P}_W = \mathbf{R}(\theta)\mathbf{P}_B + \begin{bmatrix} x \\ z \end{bmatrix}, \tag{1}$$

$$\mathbf{R}(\theta) = \begin{bmatrix} \cos\theta & \sin\theta \\ -\sin\theta & \cos\theta \end{bmatrix} \tag{2}$$

where $[x, z]^\top$ is the position of x_B-z_B axis origin in x_W-z_W axis and represents the position of the glider, θ is the angular offset between the two coordinate frames and is the pitch angle of the glider. This establishes the generalized coordinates $\mathbf{q} = [x, z, \theta]$.

Every component on the glider is assumed to have a CoM located at $[l_{gnx}, l_{gnz}]^\top$, and a CoB at $[l_{bnx}, l_{bnz}]^\top$ on the $x_B - z_B$ axis, where n is a designator for every component. For the dual buoyancy controller equipped glider, there are three components; the body which includes the fuselage and wing (n=0); the front buoyancy controller (n=1) and the rear buoyancy controller (n=2). Using Eq.1, the CoM and

CoB of any rigid body or component on the glider can be prescribed kinematically. This becomes the basis for finding the Lagrangian $L = T - U$ where T and U are the sums of kinetic and potential energies, respectively. An assumption can be made regarding the CoMs of the glider such that they can be combined into one. This is due to the fact that the mass of the buoyancy controllers are significantly smaller compared to the body so that the net effect of changing their CoM locations during expansion or contraction with respect to the composite CoM is negligible. And so, only a single point mass M representing the composite CoM is defined and located at l_{gx} and l_{gz}. By the same logic, the moment of inertia of the glider is assumed to be combined into a single parameter I. And so the kinetic and potential energy is defined to be

$$T = \frac{1}{2}M\dot{x}_G^2 + \frac{1}{2}M\dot{z}_G^2 + \frac{1}{2}I\dot{\theta}^2, \tag{3}$$

where

$$\begin{bmatrix} x_G \\ z_G \end{bmatrix} = \mathbf{R}(\theta)\begin{bmatrix} l_{gx} \\ l_{gz} \end{bmatrix} + \begin{bmatrix} x \\ z \end{bmatrix}$$

and

$$U = -Mgz_G + \rho g V_0 z_{b0} + \rho g V_1 z_{b1} + \rho g V_2 z_{b2}, \tag{4}$$

where

$$\begin{bmatrix} x_{Bn} \\ z_{Bn} \end{bmatrix} = \mathbf{R}(\theta)\begin{bmatrix} l_{bnx} \\ l_{bnz} \end{bmatrix} + \begin{bmatrix} x \\ z \end{bmatrix},$$

In Eq.4, g is gravity, ρ is the density of water and $V_{0\cdots2}$ V_2 are the volumes of the body and buoyancy controllers. Using these expressions the Larangian and subsequent Euler-Lagrange equations are easily found to be

$$\mathbf{M}(\mathbf{q})\ddot{\mathbf{q}} + \mathbf{V}(\mathbf{q},\dot{\mathbf{q}}) + \mathbf{C}\dot{\mathbf{q}} + \mathbf{G}(\mathbf{q}) = \mathbf{Q} \tag{5}$$

$$\mathbf{q} = \begin{bmatrix} x & z & \theta \end{bmatrix}^\top, \quad \mathbf{Q} = \begin{bmatrix} Q_x & Q_z & Q_\theta \end{bmatrix}^\top$$

$$\mathbf{M} = \begin{bmatrix} M & 0 & M_{13} \\ 0 & M & M_{23} \\ M_{13} & M_{23} & M_{33} \end{bmatrix}, \mathbf{V} = \begin{bmatrix} M_{23}\dot{\theta}^2 \\ -M_{13}\dot{\theta}^2 \\ 0 \end{bmatrix},$$

$$\mathbf{C} = \begin{bmatrix} 0 & 0 & 0 \\ 0 & 0 & 0 \\ 0 & 0 & C_{33} \end{bmatrix}, \mathbf{G} = \begin{bmatrix} 0 \\ -F_g + F_{b0} + F_{b1} + F_{b2} \\ (\tau_{bz} + F_g l_{gz})S_\theta + (\tau_{bx} + F_g l_{gx})C_\theta \end{bmatrix},$$

$$S_\theta = \sin\theta, C_\theta = \cos\theta, M_{13} = M(l_{gz}C_\theta - l_{gx}S_\theta),$$
$$M_{23} = -M(l_{gz}S_\theta + l_{gx}C_\theta), M_{33} = Ml_{gz}^2 + Ml_{gx}^2 + I,$$
$$F_g = Mg, F_{b0} = \rho g V_0, F_{b1} = \rho g V_1, F_{b2} = \rho g V_2,$$
$$\tau_{bz} = -F_{b0}l_{b0z} - F_{b1}l_{b1z} - F_{b_2}l_{b2z},$$
$$\tau_{bx} = -F_{b1}l_{b0x} - F_{b1}l_{b1x} - F_{b2}l_{b2x},$$

where $\mathbf{M}$, $\mathbf{V}$, $\mathbf{C}$, and $\mathbf{G}$ are the inertia, coriolis-centrifugal, damping friction and gravity matrices respectively. $\mathbf{Q}$ is the matrix of generalized forces that are the entry point of hydrodynamic forces lift and drag and the pitching moment. As shown in Fig.3b, the attack angle α is the angle between the x_B axis and the direction of flow and lift F_L and drag F_D act on the body via the center of pressure (CoP). Lift is perpendicular to the direction of flow while drag is parallel to it. Since the CoP is typically not aligned with the CoM of the glider, a pitching moment τ_θ is generated. The generalized forces are then found to be

$$\begin{bmatrix} Q_x \\ Q_z \\ Q_\theta \end{bmatrix} = \begin{bmatrix} \cos\theta & -\sin\theta & 0 \\ \sin\theta & \cos\theta & 0 \\ 0 & 0 & 1 \end{bmatrix}\begin{bmatrix} F_x \\ F_z \\ \tau_\theta \end{bmatrix} \tag{6}$$

where F_x and F_z are the forces in the x_B and z_B axes respectively. By projecting the hydrodynamic forces to the direction of these forces, Eq.6 can be written as

$$\begin{bmatrix} Q_x \\ Q_z \\ Q_\theta \end{bmatrix} = \begin{bmatrix} \cos\theta & -\sin\theta & 0 \\ \sin\theta & \cos\theta & 0 \\ 0 & 0 & 1 \end{bmatrix}\begin{bmatrix} \cos\alpha & -\sin\alpha & 0 \\ \sin\alpha & \cos\alpha & 0 \\ 0 & 0 & 1 \end{bmatrix}\begin{bmatrix} -F_D \\ -F_L \\ \tau_\theta \end{bmatrix}. \tag{7}$$

By inspection, it can easily be seen that F_{b1} and F_{b2} are represent the buoyancy generated by the buoyancy controllers. Note also that these two terms directly affect the $\ddot{z}$ and $\ddot{\theta}$ rows of Eq.5 corresponding to vertical motion and pitch control. On the other hand, horizontal motion is not directly controllable. This completes the rigid body dynamics aspect of the model and so the CFD component will follow.

B. Computational Fluid Dynamics Modeling

The use of CFD to model the hydrodynamic forces and moment was shown by Arima to converge to measured values of their glider in [12] which shows its validity. To perform the calculation, a mesh representation of the glider is needed which is generated from the CAD model of the dual buoyancy controller equipped glider shown in Fig.2b. The actual calculation was done in OpenFOAM which is a free and open source CFD software. As a preliminary CFD model, the $k-\varepsilon$ was adopted. Future endeavors will include determining whether the $k-\varepsilon$ model is appropriate by comparing the simulated results with experimental data. The setup of the simulation is shown in Fig.4a where a total of 4,149,018 cells, 12,835,948 faces and 4,543,312 points were used for the parameters of the computational domain. The calculation was performed for different angles of attack by rotating the model from 0 to 90 degrees at 5 degree intervals. Due to the symmetry of the robot about the horizontal plane, negative angles do not need to be calculated as lift and pitching moment would just be the opposite value of the corresponding positive angles while drag would be the same. Flow velocities of 0.1[m/s], 0.2[m/s] and 0.5[m/s] were used for all the different angle settings. A pressure and velocity plot is shown in Fig.4b for angles of attack equal to 0, 30, 60 and 90 degrees at 0.1[m/s]. The results of the CFD simulation can be seen in Fig.5 where the lift and drag forces as well as the pitching moment for 0.1, 0.2 and 0.5 [m/s] are shown in Fig.5a, c and e. In Fig.5b,d and f, the forces and moment values are divided by the square of the corresponding flow velocities. The results are in accordance with the relationship established by Eq.8 below.

$$F_L = C_L\frac{1}{2}\rho S v^2, F_D = C_D\frac{1}{2}\rho S v^2, \tau_\theta = C_\theta\frac{1}{2}\rho S v^2, \tag{8}$$

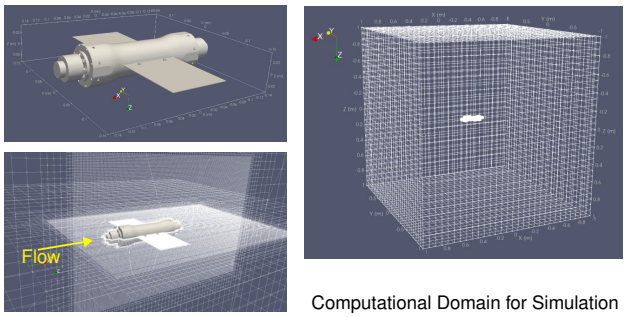

(a) Computational Fluid Dynamics using OpenFOAM for the dual buoyancy controller equipped glider

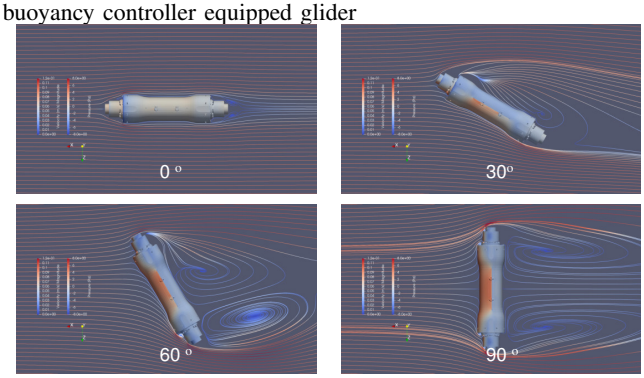

(b) Pressure an velocity plot of CFD simulation at different angles for 0.1[m/s] flow velocity

Fig. 4: CFD simulation parameters and example simulation results

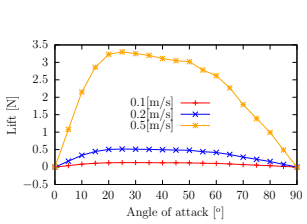

(a) Lift-α

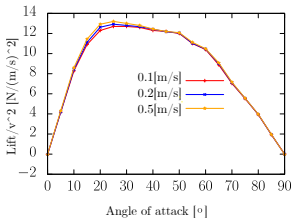

(b) Lift-α normalized to v^2

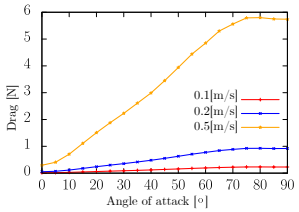

(c) Drag-α

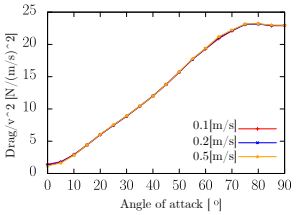

(d) Drag-α normalized to v^2

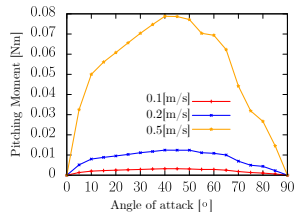

(e) Moment-α

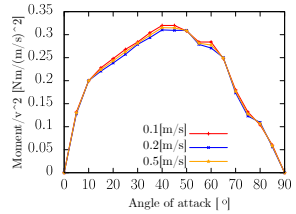

(f) Moment-α normalized to v^2

Fig. 5: Results of CFD for lift,drag and pitching moment

where v is the flow velocity, S is the projected area of the body in the direction of the flow, C_L, C_D and C_θ are the lift, drag and moment coefficients.

Although the coefficients C_L, C_D and C_θ can be calculated from Eq.8, this is not necessary as calculation of forces and moment is needed instead. Lift F_L, drag F_D and torque τ_θ are calculated as $F_L = P_{F_L}(\alpha)v^2$, $F_D = P_{F_D}(\alpha)v^2$ and $\tau_\theta = P_{\tau_\theta}(\alpha)v^2$, respectively. P_{F_L}, P_{F_D} and P_{τ_θ} are 5th, 4th, 7th degree polynomials fitted to the data in Fig.5 b, d and e, respectively. Using these, the high computational cost of CFD can be averted allowing faster calculation of each time step of the simulation.

C. Calculating volume of the buoyancy controller

The bellows based buoyancy controller is able to change its volume since the pleats of the bellows deform. Actual deformation may exhibit nonlinear behavior especially under higher pressures and should be determined through proper measurement. However, for the current target of lower depth testing, pressure is also lower and so the deformation can be assumed to be close to linear. To calculate the volume of the buoyancy controller, a simple geometric model was developed. As shown in Fig.6, the buoyancy controller is

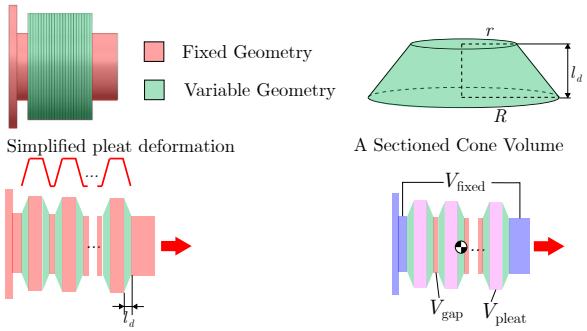

Fig. 6: Volume calculation of the bellows type buoyancy controller

assumed to have a part that has a fixed geometry and a variable geometry part. The variable geometry part can be assumed to form a sectioned cone that has height l_d. As a result, the total volume of the buoyancy controller is expressed as

$$V_{1,2} = V_{\text{fixed}} + m_p V_{\text{pleat}} + m_p V_{\text{gap}} + 2m_p V_d(l_d) \tag{9}$$

$$V_d(l_d) = \frac{1}{3}\pi l_d \left(r^2 + rR + R^2\right)$$

$$l_d = \frac{L_{\text{total}}}{m_p} \tag{10}$$

where m_p is the number of pleats and L_{total} is the total amount of extension of the buoyancy controller.

III. Simulation Architecture and Preliminary Results

The architecture of the simulation is shown in Fig.7 where the input of the entire simulation is the volume of each buoyancy controller via their corresponding amount of extension

TABLE II: Simulation Parameters

symbol	unit	value
M	[kg]	0.787
I	[kgm^2]	0.029
l_{gx}, l_{gz}	[m]	0, 0.001
V_0	[m^3]	0.787x10^{-3}
C_{33}	[Nms]	0.001
g	[m/s^2]	9.8

in millimeters. The nonlinear state space equations based on Eq.5 calculates the accelerations which are numerically integrated using a fourth degree Runge-Kutta function. The resulting velocity and position values are used to calculate

$$\alpha = \tan^{-1}\left(\frac{\dot{z}}{\dot{x}}\right) + \theta, \tag{11}$$

$$v^2 = \dot{x}^2 + \dot{z}^2, \tag{12}$$

where the expression $\tan^{-1}\left(\frac{\dot{z}}{\dot{x}}\right)$ determines the instantaneous flow in the water which makes the assumption that the water is still and the glider moves through it. This assumption may hold true in practical situations so long as the glider moves slowly and the water starts from a still state at the start of gliding.

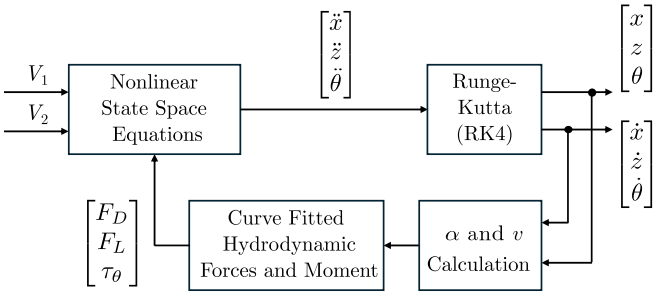

Fig. 7: Simulation Block Diagram

A. *Preliminary Results*

Preliminary results of simulations using the process described in Fig.7 and parameters like mass, CoM position were measured and applied to the simulation as shown in Table II. Simulation based on actual gliding where the front buoyancy controller was first contracted resulting in downward gliding motion for 10 [s] followed by expansion which causes upward gliding motion was programmed. In Fig.8, the results of the simulation are shown. The figure shows snapshots at different timestamps of actual gliding with the simulation trajectory in magenta is overlayed to show a certain degree of adherence between the two. Also, snapshots of the 2D animation of the glider simulation drawn in a flat 2D representation at similar timestamps are overlayed with the actual glider which also shows similar behavior for pitching performance. This simulation is not yet optimized as some other parameters still need to be tuned further. Nevertheless, it shows the validity and promise of the proposed approach in capturing the intricacies of gliding motion.

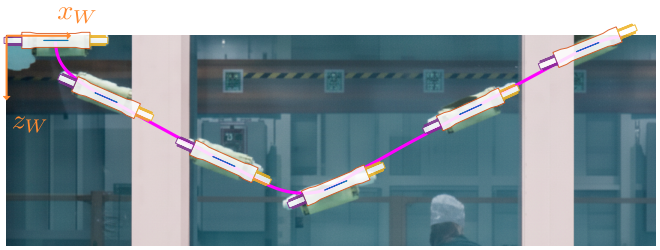

Fig. 8: Preliminary Simulation Results and Comparison

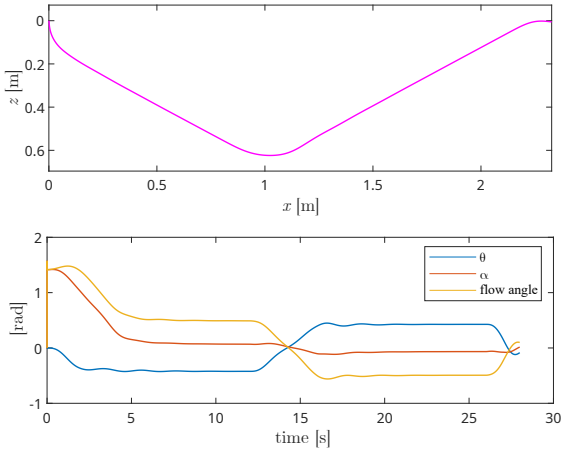

Fig. 9: Simulation Results for trajectory and pitch, attack and flow angle

IV. Summary and Future Work

The authors proposed an approach that utilizes the parametric nature of Lagrangian Mechanics to enable multi buoyancy controller equipped glider design coupled with an exhaustive CFD calculation that was simplified through curve fitting to deliver a promising simulation method. Further testing of the simulation will be performed with a more involved comparison of not only trajectory but pose and position. The results also open up the possibility of exploring new control techniques rapidly.

References

[1] Y. SARUTA, T. OMURO, and T. TAKAHASHI, "Development of a small and modular underwater robot for lakes and marshes surveying : Development of prototype main module and basic investigation," in *The Proceedings of JSME annual Conference on Robotics and Mechatronics (Robomec)*, vol. 2012, no. 0, may 2012, pp. 2P1–I11.

[2] S. TAKANOHASHI, S. IGARASHI, and T. TAKAHASHI, "1A1-H07 Development of a small and modular UROV for environmetntal surveying : Implementation and evaluation of an undisturbed soil core sampling module(Underwater Robot and Mechatronics (1))," *The Proceedings of JSME annual Conference on Robotics and Mechatronics (Robomec)*, vol. 2014, no. 0, pp. 1A1–H07, 2014.

[3] K. ANZAI and T. TAKAHASHI, "2A1-E07 Development of a small and modular UROV for environmental surveying : Improvement of an undisturbed soil core sampling module," in *The Proceedings of JSME annual Conference on Robotics and Mechatronics (Robomec)*, vol. 2015, no. 0. The Japan Society of Mechanical Engineers, 2015, pp. 2A1–E07.

[4] A. Khan, P. Borja, D. Bazazian, M. Hisham, B. Nordin, E. Petritoli, and F. Leccese, "Autonomous Underwater Glider: A Comprehensive Review," *Drones 2025, Vol. 9, Page 21*, vol. 9, no. 1, p. 21, dec 2024. [Online]. Available: https://www.mdpi.com/2504-446X/9/1/21/htm https://www.mdpi.com/2504-446X/9/1/21

[5] C. P. Jones, "Slocum glider persistent oceanography," *2012 IEEE/OES Autonomous Underwater Vehicles, AUV 2012*, 2012.

[6] L. Cooney, "Expanding the capabilities of the Slocum glider," *OCEANS 2016 MTS/IEEE Monterey, OCE 2016*, nov 2016.

[7] K. NAKATA and T. TAKAHASHI, "Development of a buoyancy controller using bellows for environmental surveying underwatar robot -Fabrication of PTFE bellows telescopic mechanism that can be operated under high water pressure-," in *The Proceedings of JSME annual Conference on Robotics and Mechatronics (Robomec)*, vol. 2025, Yamagata, 2025, pp. 2P1–I02.

[8] H. Inami, T. Takahashi, and F. Dai-ich, "1 2011," in *The Proceedings of JSME annual Conference on Robotics and Mechatronics (Robomec)*, 2024, pp. 2P2–C01.

[9] J. Huang, H.-S. Choi, D.-W. Jung, J.-H. Lee, M.-J. Kim, K.-B. Choo, H.-J. Cho, H.-S. Jin, C. . Huang, J. . Choi, H.-S. . Jung, D.-W. . Lee, J.-H. . Kim, M.-J. . Choo, K.-B. . Cho, H.-J. . Jin, and H.-S. Design, "Design and Motion Simulation of an Underwater Glider in the Vertical Plane," *Applied Sciences 2021, Vol. 11, Page 8212*, vol. 11, no. 17, p. 8212, sep 2021.

[10] N. Mahmoudian and C. Woolsey, "Underwater glider motion control," *Proceedings of the IEEE Conference on Decision and Control*, pp. 552–557, 2008.

[11] J. Sherman, R. E. Davis, W. B. Owens, and J. Valdes, "The autonomous underwater glider "Spray"," *IEEE Journal of Oceanic Engineering*, vol. 26, no. 4, pp. 437–446, oct 2001.

[12] M. Arima, N. Ichihashi, and T. Ikebuchi, "Motion characteristics of an underwater glider with independently controllable main wings," *OCEANS'08 MTS/IEEE Kobe-Techno-Ocean'08 - Voyage toward the Future, OTO'08*, 2008.